

Catalytic conversions of chloroolefins over iron oxide nanoparticles

2.* Isomerization of dichlorobutenes over iron oxide nanoparticles stabilized on the surface of ultradispersed poly(tetrafluoroethylene)

T. N. Rostovshchikova,^a M. S. Korobov,^b D. A. Pankratov,^a G. Yu. Yurkov,^{b*} and S. P. Gubin^b

^aDepartment of Chemistry, M. V. Lomonosov Moscow State University,
1 Leninskie Gory, 119992 Moscow, Russian Federation.

Fax: +7 (095) 932 8846. E-mail: rtn@kinet.chem.msu.ru

^bN. S. Kurnakov Institute of General and Inorganic Chemistry, Russian Academy of Sciences,
31 Leninsky prosp., 119991 Moscow, Russian Federation.

Fax: +7 (095) 954 1279. E-mail: gubin@igic.ras.ru; gy_yurkov@mail.ru

Nanosized iron oxides stabilized on the surface of ultradispersed poly(tetrafluoroethylene) (UPTFE) granules were synthesized by the thermal destruction of iron formate in boiling bed of UPTFE on the surface of heated mineral oil. The particle size of nanoparticles (~6 nm) containing 5, 10, and 16 wt.% Fe depends weakly on the temperature of synthesis and iron to polymer ratio. The metal state is determined by the synthesis conditions. The nanoparticles synthesized at 280 °C consist mainly of the Fe₃O₄ and Fe₂O₃ phases. The samples obtained at 320 °C also contain iron(II) oxide. The catalytic properties of the obtained samples were tested in dichlorobutene isomerization. Unlike isomerization on the iron oxide nanoparticles supported on silica gel, reaction over the UPTFE supports proceeds without an induction period. The sample with 10 wt.% Fe containing magnetically ordered γ -Fe₂O₃ nanoparticles possesses the highest catalytic activity. Fast electron exchange between the iron ions in different oxidation states and high defectiveness of the nanoparticles contribute, most likely, to the catalytic activity.

Key words: nanosized iron oxide, ultradispersed poly(tetrafluoroethylene), catalysis, nanoparticles, nanosized supports, dichlorobutene isomerization, catalysis by nanoparticles.

Nanosized iron oxides stabilized on silicas or in the volume of polymer matrix serve as active and selective catalysts of halogenolefin conversions.^{1,2} The key factors determining specific features of nanoparticles are their size and simultaneous presence of iron species in two charge states in the active phase of the catalyst. Iron oxide nanoparticles supported by silicas are characterized by a strong dependence of the catalyst composition on the iron to support ratio, silica structure, particle size, and specific features of their distribution on the support. Polymeric matrices are successfully used to stabilize metallic and metal oxide nanoparticles rather uniform in size.^{3–5} The purpose of this work is to compare the catalytic properties of the iron-containing nanoparticles stabilized on the surface of ultradispersed poly(tetrafluoroethylene) (UPTFE) with those of the earlier studied catalysts based on iron oxides and stabilized on silicas¹ or in the polyethylene volume.² UPTFE was chosen as a polymeric stabilizing matrix, because its surface can uniformly be covered with metal-containing nanoparticles by the thermolysis of metal-containing compounds.^{6,7} This material shows

the well developed surface, mechanical strength, and resistance of UPTFE and related nanocomposites to aggressive media. Metal-containing nanoparticles are stabilized not inside but on the surface of matrix and easily accessible to reactants. Accordingly, the material seems to be a promising support for the preparation of nanosized catalysts, especially for their use in fluid bed.

Experimental

Composite materials consisting of metal-containing nanoparticles stabilized on the surface of UPTFE were synthesized by the thermal destruction of the metal-containing compound in a dispersion system UPTFE—mineral oil.^{6,7} Iron(III) formate (Fe(HCOO)₃) was used as the main metal-containing precursor. In addition, samples were obtained by the thermolysis of iron pentacarbonyl Fe(CO)₅. The metal-containing precursor was decomposed in an inert atmosphere at 280–320 °C. The flow rate of the inert gas (argon) used for nanoparticle synthesis was controlled in a way to ensure the fast and complete removal of volatile decomposition products of the precursor and solvent from the reactor. Due to a small size (150–500 nm), UPTFE nanogranules form a "fluid" bed above the surface of heated mineral oil.^{6,7} This regime provides a uniform distribution of

* For Part 1, see Ref. 1.

forming metal-containing nanoparticles over the nanogranule surface. With an increase in the number of the metal-containing nanoparticles on the UPTFE surface, the weight of the nanogranules increases and they leave the zone of nanoparticle formation in the fluid bed and enter the oil. The oil from a formed dark precipitate was washed off with benzene in a Soxhlett apparatus, and solvent residues were removed *in vacuo*. The samples were stored in air. The produced materials were finely dispersed powders, whose color turned from gray to black, depending on the metal-containing phase concentration.

The iron concentration in the polymer was varied from 4 to 16 wt.%, and its content in the prepared samples was determined by elemental analysis.

The particle size was determined by transmission electron microscopy (TEM) on a JEM-100B setup (JEOL). For this examination, the material under study was ultrasonicated in an aqueous-alcohol solution, and a droplet of the resulting suspension was introduced on a copper support covered with carbon.

The compositions of the starting catalysts were determined by Mössbauer spectroscopy. Absorption Mössbauer spectra were recorded on an MS1101E electrodynamic-type spectrometer (MNPP "MosTek") at room temperature. Isotope ^{57}Co in the metallic rhodium matrix with an activity of 1 mCi (ZAO "Tsiklotron") was used as a γ -radiation source. Isomeric shifts were determined relatively to α -Fe. Spectra were processed by the standard least-squares method assuming the Lorentz lineshape and using the UNIVEM v.4.50 program.

3,4-Dichlorobut-1-ene (3,4-DCB) was isomerized in sealed glass ampules with stirring in a temperature interval of 70–100 °C in the presence of oxygen.¹ 3,4-DCB (0.1–0.2 mL, $(1\text{--}2)\cdot 10^{-3}$ mol) and catalyst ($0.005\text{--}0.01$ g, $(0.5\text{--}3)\cdot 10^{-5}$ moles of iron) were used. The composition of the reaction mixture was determined on an LKhM-3700 chromatograph with the SE-30 stationary phase at 100 °C. The main product of 3,4-DCB isomerization is *trans*-1,4-dichlorobut-2-ene (*trans*-1,4-DCB). The yield of the *cis*-isomer and by-products did not exceed 2–3%.

Specific catalytic activity and isomerization rate constants were used as measures of catalytic activity. The specific catalytic activity (A_{sp}) was calculated from the initial isomerization rate as a ratio of the molar amount of *trans*-1,4-DCB formed within 1 h to the iron content in the sample. The isomerization rate constants of the first order with respect to 3,4-DCB were determined by the linearization of kinetic curves of *trans*-1,4-DCB accumulation in the coordinates of the first-order reversible reaction $\ln[A_{\infty}/(A_{\infty} - A)] - t$, where A_{∞} is the equilibrium concentration of *trans*-1,4-DCB, and A is its current concentration.¹ Based on the found rate constants of the forward (k_1) and backward (k_{-1}) isomerization reactions of the first order with respect to 3,4-DCB, apparent rate constants of the second order with respect to the reactant and catalyst were calculated

$$k_2 = k_1/[\text{Fe}].$$

The obtained values were independent of the iron concentration in the reaction mixtures.

Apparent activation energies of isomerization were determined from the temperature dependence of the rate constants of the forward and backward reactions (k_2 and k_{-2} , respectively) in the 70–100 °C range.

Results and Discussion

Particle size. Under electron beam UPTFE nanogranules look like almost planar spheres with diffuse boundaries (Fig. 1). When iron-containing particles were dispersed on a support, the sample contains poly(tetrafluoroethylene) granules of approximately the same sizes as in the UPTFE powder with the only distinction that dark spherical aggregates (metal-containing nanoparticles) are observed on their surface.

The average diameter of the metallic particles (d) depends slightly on the conditions of synthesis, and the

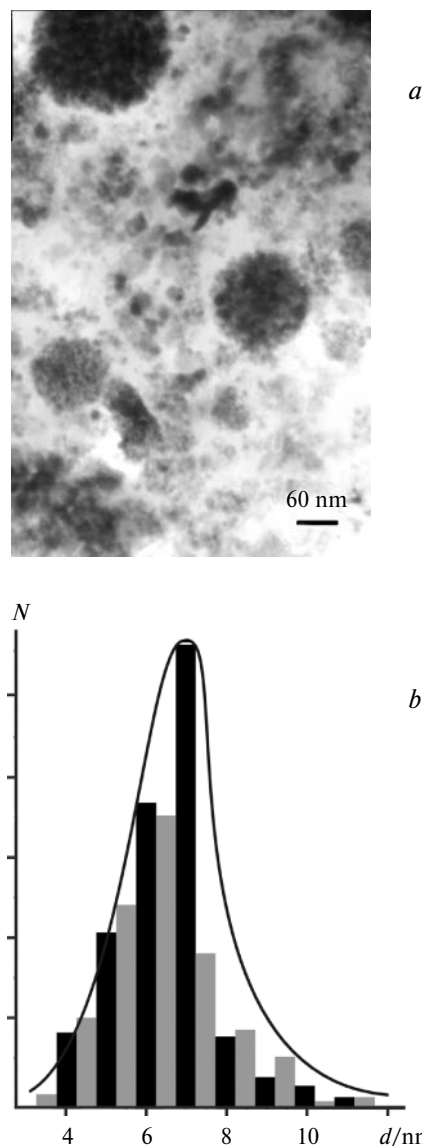


Fig. 1. TEM microphotograph of the iron-containing nanoparticles (6.5 ± 1.5 nm) stabilized on the UPTFE surface (a) and the size distribution diagram (b) for sample 4 with an iron content of 10.3 wt.% (N is the number of particles, and d is their diameter).

Table 1. Results of mathematical processing of the TEM microphotographs and Mössbauer spectra of samples 1–4 with different iron contents (see Figs 1 and 2)

Sample	[Fe] (wt.%)	<i>d</i> /nm	Sub- spectrum	δ		B_{hf} /kOe	Γ_{exp} /mm s ⁻¹	<i>S</i> (%)
				Δ mm s ⁻¹				
Temperature of synthesis 280 °C								
1	4.7	5.0	1	0.37±0.02	-0.02±0.04	480.6±1.5	0.64±0.08	19
	4.7	5.0	2	0.56±0.03	-0.02±0.05	434.7±2.8	1.13±0.12	32
	4.7	5.0	3	0.34±0.02	0.85±0.03	—	0.55±0.04	15
	4.7	5.0	4	1.23±0.01	1.65±0.03	—	0.70±0.05	21
	4.7	5.0	5	1.38±0.01	2.76±0.01	—	0.21±0.01	13
2	10.1	6.5	1	0.31±0.01	-0.01±0.01	504.4±0.2	0.38±0.01	23
	10.1	6.5	2	0.63±0.01	0.01±0.01	472.6±0.5	0.59±0.02	39
	10.1	6.5	3	0.62±0.01	0.07±0.03	442.7±1.8	0.63±0.08	12
	10.1	6.5	4	0.70±0.20	0.08±0.04	404.3±2.0	0.54±0.10	6
	10.1	6.5	5	0.30±0.01	0.99±0.02	—	0.54±0.03	6
	10.1	6.5	6	1.40±0.01	2.85±0.01	—	0.29±0.01	14
3	16.3	6.0	1	0.38±0.01	-0.22±0.01	510.4±0.4	0.34±0.01	11
	16.3	6.0	2	0.32±0.01	-0.09±0.01	485.0±0.6	0.52±0.02	16
	16.3	6.0	3	0.58±0.01	-0.01±0.01	450.9±0.8	0.85±0.04	24
	16.3	6.0	4	0.63±0.02	0.00±0.01	396.7±2.8	1.10±0.08	11
	16.3	6.0	5	1.29±0.01	2.42±0.02	—	1.44±0.03	20
	16.3	6.0	6	1.35±0.01	2.80±0.01	—	0.25±0.01	18
Temperature of synthesis 320 °C								
4	10.3	6.5	1	0.29±0.01	-0.01±0.01	480.7±0.3	0.39±0.02	13
	10.3	6.5	2	0.56±0.01	0.01±0.01	446.7±0.5	0.76±0.03	30
	10.3	6.5	3	0.64±0.02	-0.03±0.04	391.4±2.7	1.26±0.12	15
	10.3	6.5	4	0.42±0.02	0.89±0.03	—	0.74±0.02	19
	10.3	6.5	5	1.11±0.02	2.36±0.04	—	0.94±0.02	23

Note. *d* is the average particle diameter, δ is the isomeric shift, Δ is the quadrupole shift, B_{hf} is the magnetic field, Γ_{exp} is the linewidth, and *S* is the relative subspectrum surface area.

mean size deviation does not exceed 30%. The results of calculation of the average particle deviation for the samples studied are presented in Table 1. It has previously⁷ been shown that the particle size is also ~6 nm when iron carbonyl is used as a precursor.

Nanoparticle composition. According to the data of Mössbauer spectroscopy, the tested composites synthesized by the thermal destruction of iron(III) formate contain iron in several different states, as the most part of similar materials.^{3–5} When UPTFE is used as a stabilizing matrix, the formation of fluoro-substituted iron derivatives can be expected along with oxygen compounds.^{6,7} Taking into account a possible presence of mixed iron fluorooxo compounds, similar parameters of the Mössbauer spectra, and relaxation effects for nanosized objects, we cannot interpret unambiguously some spectral components, and the interpretation given should be considered only as the most probable one.

The Mössbauer spectra of samples 1–4 and the corresponding parameters are presented in Fig. 2 and Table 1. The property common for all samples is the presence of magnetically ordered Fe₃O₄ (subspectra 1 and 2 for samples 1 and 4, subspectrum 2 for sample 2, and subspectra 2 and 3 for sample 3). Despite a large linewidth

(Γ_{exp}) of these sextets, it can be noted that crystallites formed in samples 1 and 3 are evidently less defect than those in sample 2 synthesized under the same conditions. This follows from the fact that the valent state of the iron atoms in the Fe₃O₄ sublattices cannot be distinguished in the spectrum of sample 2. As a rule, Mössbauer spectra of Fe₃O₄ with the structure of inverse spinel are described by the superposition of three subspectra as sextets: one sextet with an isomeric shift of 0.28–0.34 mm s⁻¹ corresponding to the iron(III) atoms in the tetrahedral environment (magnetic field at 300 K $B_{\text{hf}} = 485–495$ kOe)⁸ and two subspectra with isomeric shifts in an interval of 0.60–0.68 mm s⁻¹ corresponding to the Fe^{II} and Fe^{III} ions ($B_{\text{hf}} = 450–460$ kOe), which are located in octahedral gaps involving in fast electron exchange. However, in sample 2, unlike samples 1, 3, and 4, no subspectrum with an isomeric shift of 0.28–0.34 mm s⁻¹ is detected. Evidently, the tetrahedral gaps in the Fe₃O₄ nanoparticles of sample 2 remained unfilled because of defect nature of particles, which results in the disappearance of the corresponding magnetic sublattice. In addition, the spectrum of sample 2 distinctly shows subspectrum 1 characteristic of more oxidized iron oxide (γ -Fe₂O₃)⁸ with the spinel superstructure. In the latter, the tetrahedral sub-

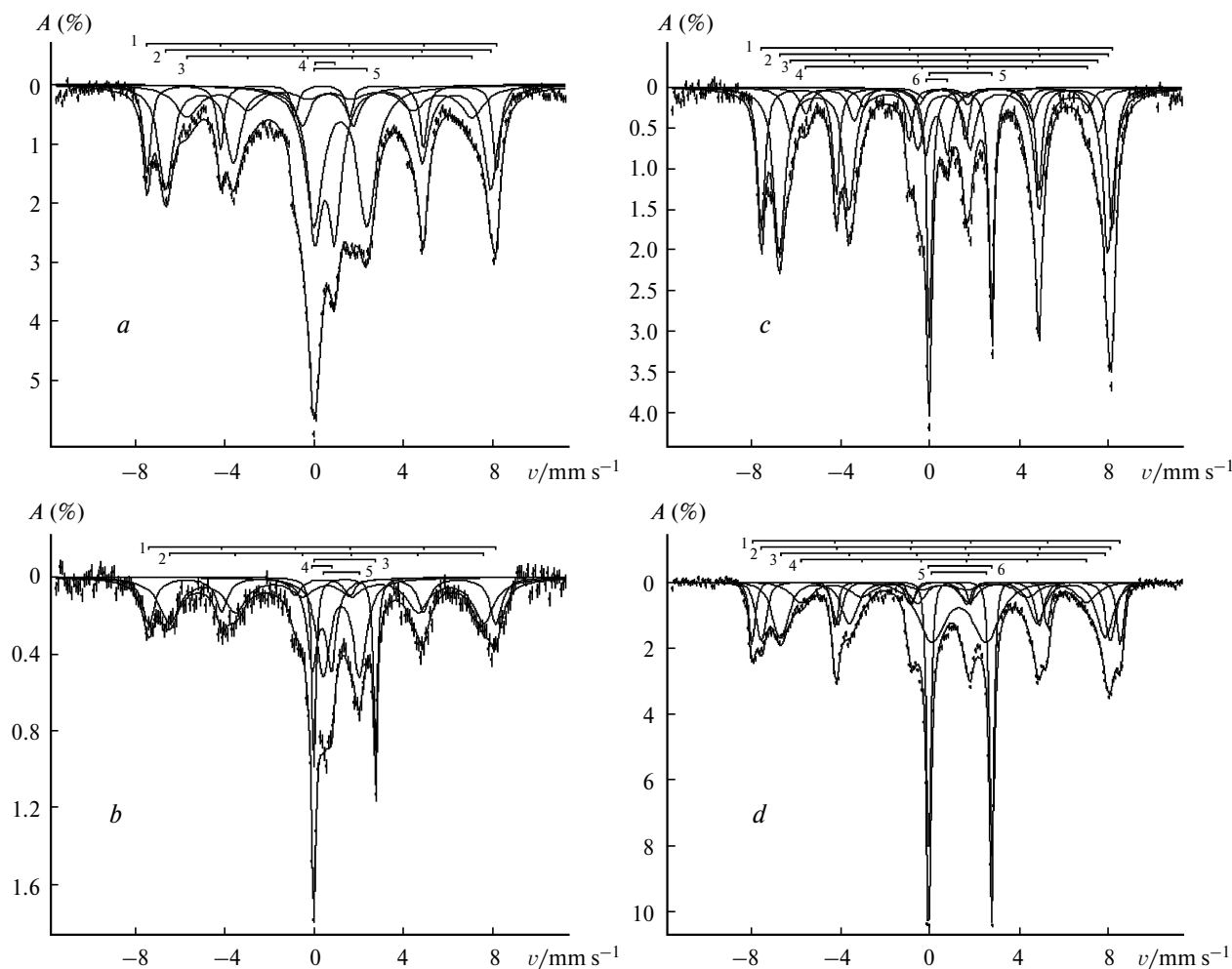


Fig. 2. Mössbauer spectra of the iron-containing nanoparticles supported in the UPTFE surface by the thermal destruction of iron formate at 320 (a) and 280 °C (b–d); iron content 10.3 (sample 4) (a), 4.7 (sample 1) (b), 10.1 (sample 2) (c), and 16.3 wt.% (sample 3) (d); v is the rate of the γ -radiation source.

lattice is filled completely, 4/3 positions of the octahedral sublattice are filled with iron(III) ions, and 8/3 positions are vacant. That is why, probably, nanosized particles have a complex spinel-based structure including γ - Fe_2O_3 and Fe_3O_4 and are highly defective.

The spectrum of sample 3 with the maximum iron content has rather narrow ($\Gamma_{\text{exp}} = 0.34 \text{ mm s}^{-1}$) magnetically split lines (see Fig. 2, d and Table 1, subspectrum 1, $B_{\text{hf}} = 510.4 \text{ kOe}$), which are attributed to a highly crystalline α - Fe_2O_3 .⁸ The other magnetically split subspectra in all samples are assigned to the iron ions on the nanoparticle surface or in nanoparticles of a smaller size.

The spectrum of sample 1 with a low iron content exhibits a resonance signal as a doublet (subspectrum 3) with $\delta = 0.34 \text{ mm s}^{-1}$. A similar doublet, although less intense, is observed for the spectrum of sample 2 (subspectrum 5). This indicates that samples 1 and 2 contain iron(III) oxide in the superparamagnetic state, while

superparamagnetic Fe_2O_3 is not virtually detected in the spectra of samples 3 and 4.

Broad doublet lines with $\delta = 1.34$ – 1.40 mm s^{-1} or $\delta = 1.23$ – 1.29 mm s^{-1} , which are observed in the spectra of samples 1–3 (see Fig. 2, b–d), are attributed, most likely, to iron(II) fluoro-substituted derivatives, for example, FeF_2 , or to crystal hydrates of iron(II) fluoride,⁹ respectively.

The most striking distinctive feature of sample 4 (see Fig. 2, a) synthesized at 320 °C is the absence of a narrow doublet component with the isomeric shift value corresponding to iron(II) fluoride compounds. Unlike other samples, a broad doublet with $\delta = 1.11 \text{ mm s}^{-1}$ is observed (subspectrum 5), which can be assigned to the iron(II) atoms in the octahedral oxygen environment, for example, to a nanosized oxide similar to FeO . The other spectral components of this sample can be assigned to the nanosized Fe_3O_4 particles. The most part of them is de-

scribed by subspectra 1 and 2 with somewhat lower magnetic fields on the atoms, which is characteristic of nanoparticles. Subspectrum 3 has a considerable linewidth and a small relative surface area and characterizes, evidently, the atoms on the surface of Fe_3O_4 particle. The doublet of subspectrum 4 corresponding to smaller crystallites can be ascribed to the same substance but in the superparamagnetic state. Taking into account the probability of fluoride formation during the synthesis, we cannot exclude that this component is attributed to an iron(III) oxofluoro-substituted derivative in the octahedral environment.¹⁰

Thus, the method proposed for the synthesis of iron oxide nanoparticles by iron formate thermolysis in the presence of UPTFE makes it possible to stabilize nanoparticles with similar sizes but containing iron atoms in different environments on the polymer surface. In all cases, the main phase of nanoparticles is Fe_3O_4 . An increase in the temperature of formation decomposition produces samples with a higher degree of reduction containing iron(II) oxides. Nanoparticles synthesized at a lower temperature are oxidized to a higher extent and in addition contain iron(III) oxides, whose state changes from superparamagnetic to magnetically ordered $\gamma\text{-Fe}_2\text{O}_3$ or $\alpha\text{-Fe}_2\text{O}_3$ with an increase in the metal content in the polymer.

Another substantial feature of the nanoparticles synthesized at lower temperatures is the appearance of the iron fluoride phase in the composition of nanoparticles, which has previously been observed for nanocomposites obtained in a similar way using UPTFE and iron pentacarbonyl as a metal-containing precursor. In this case, the nanoparticles contained iron carbides and $\alpha\text{-Fe}$ in addition to the oxide and fluoride phases.⁷ According to the known model,⁷ the nanoparticles are multilayer solids, a fraction of their surface contacting with polymeric support is covered with an iron fluoride layer, whereas surface areas not interacting with the polymer are covered with oxide.

Catalytic properties of iron oxides stabilized on the UPTFE surface. The specific catalytic activity of different iron-containing polymeric UPTFE-based nanocomposites in 3,4-DCB isomerization to *trans*-1,4-DCB at 100 °C (Table 2) was compared with the data for nanocomposites obtained with low-density polyethylene (LDPE) as a stabilizing matrix.² It is seen that iron-containing salts of carboxylic acids are the best precursors for synthesis of catalytically active nanoparticles. A lower activity of the samples prepared from iron carbonyls is due to the presence of the catalytically inert iron carbide phase.² The use of the UPTFE matrix for nanoparticle stabilization provides more active catalysts, which can be due to both easier accessibility of nanoparticles located on the surface rather than in the bulk support and differences in the size and composition of the particles. In the earlier⁵ described nanocomposites, the average particle size in the LDPE matrix corresponded to 15 nm, and $\gamma\text{-Fe}_2\text{O}_3$ was the main iron-containing phase. The isomerization rate on these catalysts at temperatures below 100 °C was low.

The particles stabilized on UPTFE are comparable in activity with the iron oxide particles immobilized on silicas.¹ However, the induction period for *trans*-1,4-DCB formation, which is characteristic of iron oxide nanoparticles immobilized on the silica gel surface, is not observed in the presence of the iron-containing particles on UPTFE. As in the case of iron oxides supported on the oxide supports,¹ the isomerization can formally be described by a kinetic equation of the reversible reaction of the first order with respect to 3,4-DCB. This is indicated by the kinetic curves linearized in the corresponding coordinates (Figs 3 and 4). The kinetic data in Fig. 3 concern samples 1–3 prepared under the same conditions at a destruction temperature of 280 °C. As can be seen from a comparison of curves 3 and 3' (see Fig. 3), the linear character of the dependence is retained when the amount of the catalyst used decreases. The kinetic data obtained at 70 and 80 °C for sample 4, synthesized at higher tem-

Table 2. Specific catalytic activity (A_{sp} /mole of *trans*-1,4-DCB (mol Fe)⁻¹ h⁻¹) of the iron-containing polymeric composites in 3,4-DCB isomerization

Catalyst /support	Precursor	Weight of catalyst/g	Volume of 3,4-DCB/mL	<i>t</i> /min	Yield of 1,4-DCB (%)	A_{sp}
4.7 wt.% Fe/UPTFE	$\text{Fe}(\text{HCOO})_3$	0.005	0.1	30	60	260
10.1 wt.% Fe/UPTFE	$\text{Fe}(\text{HCOO})_3$	0.005	0.2	30	61	250
16.3 wt.% Fe/UPTFE	$\text{Fe}(\text{HCOO})_3$	0.005	0.2	30	67	170
10.3 wt.% Fe/UPTFE	$\text{Fe}(\text{HCOO})_3$	0.005	0.1	30	63	130
5 wt.% Fe/LDPE	$\text{Fe}(\text{HCOO})_3$	0.01	0.1	30	58	113 ²
5 wt.% Fe/LDPE	$\text{Fe}(\text{AcO})_3$	0.006	0.1	60	65	112 ²
4.1 wt.% Fe/UPTFE	$\text{Fe}(\text{CO})_5$	0.01	0.1	30	43	110
14 wt.% Fe/UPTFE	$\text{Fe}(\text{CO})_5$	0.01	0.1	30	44	30
5 wt.% Fe/LDPE	$\text{Fe}(\text{CO})_5$	0.01	0.1	60	10	452

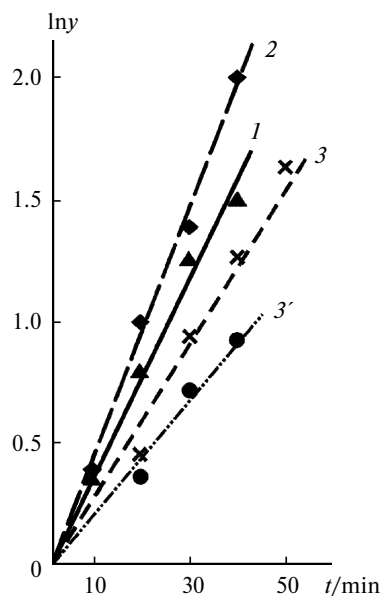


Fig. 3. Kinetic curves of *trans*-1,4-DCB accumulation in the presence of samples 1–3 (80 °C, [3,4-DCB] = 9.2 mol L⁻¹) in the coordinates $\ln y-t$ ($y = A_{\infty}/(A_{\infty} - A)$): [Fe] = 0.089 (1, 2), 0.13 (3), and 0.08 mol L⁻¹ (3'). Numbers of curves correspond to the numbers of samples.

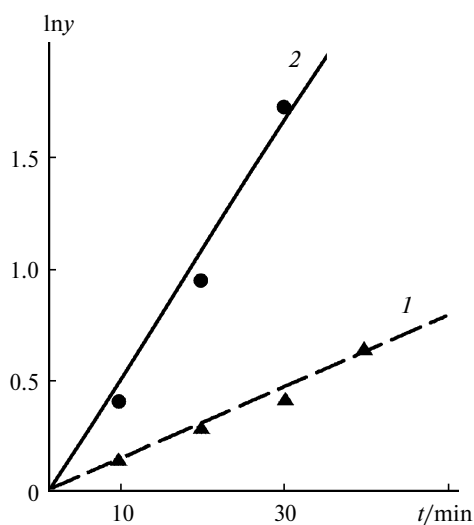


Fig. 4. Kinetic curves of *trans*-1,4-DCB accumulation in the presence of sample 4 ([3,4-DCB] = 9.2 mol L⁻¹, [Fe] = 0.18 mol L⁻¹) in the coordinates $\ln y-t$ ($y = A_{\infty}/(A_{\infty} - A)$) at 70 (1) and 80 °C (2).

perature (320 °C) than samples 1–3 are shown in Fig. 4. It is seen that the dependence is linear in this case as well. The observed rate constants of the forward and backward reactions (k_1 and k_{-1} , respectively) determined under different conditions are collected in Table 3.

It is seen that the constants depend on both the composition and method of preparation of the catalyst and the iron content in reaction mixtures. To take into account

different iron contents in different experiments, we assumed that the reaction rate and observed rate constants of the first order with respect to reactant are linear functions of the iron concentration. The apparent rate constants of the second order (k_2 and k_{-2}) calculated assuming a linear dependence of the isomerization rate on the iron concentration are also given in Table 3. It is seen that these values are almost independent of the iron content. This confirms the assumption that the reaction rate is described satisfactorily by a kinetic equation of the second order and depends linearly on the concentrations of 3,4-DCB and iron. Based on the temperature plot of the average rate constants of the second-order reaction k_2 and k_{-2} (Fig. 5), we estimated the apparent activation energies of the forward (E_2) and backward (E_{-2}) reactions

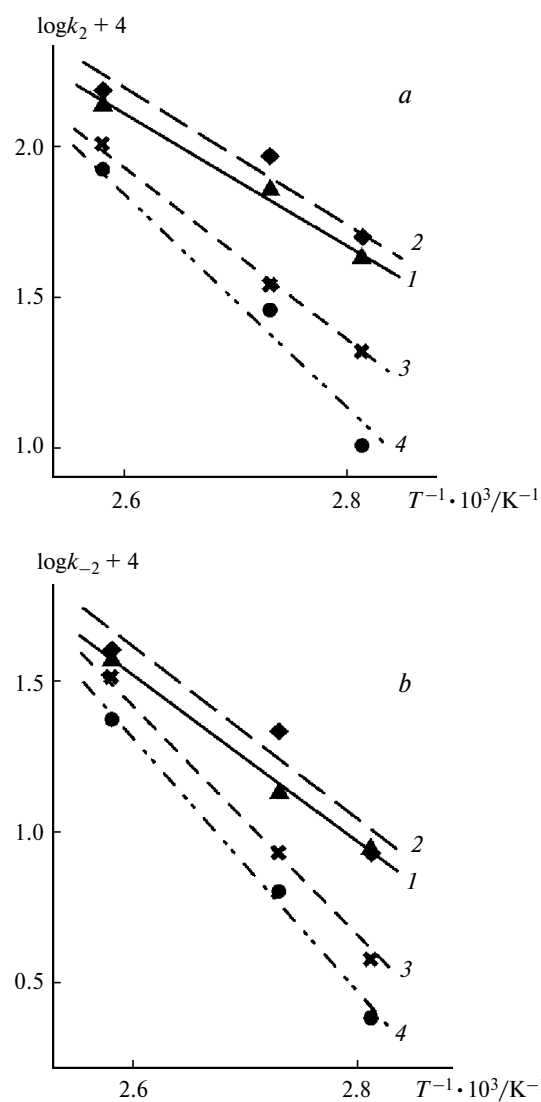


Fig. 5. Rate constants of the forward (a) and backward (b) second-order reactions (k_2 and k_{-2} , respectively) for samples 1–4 in the Arrhenius coordinates. Numbers of curves correspond to the numbers of samples.

Table 3. Rate constants of the forward and backward reactions of the first and second orders of 3,4-DCB isomerization to *trans*-1,4-DCB (k_1 , k_{-1} , k_2 , and k_{-2} , respectively) for samples 1–4

Sample*	$T/^\circ\text{C}$	[Fe]** /mol L ⁻¹	$(k_1 + k_{-1}) \cdot 10^4$	$k_1 \cdot 10^4$		k_2	
				s ⁻¹		L mol ⁻¹ s ⁻¹	
1 (4.7)	100	0.045	8.4	6.5	1.9	0.014	0.004
	80	0.022	1.6	1.3	0.3	0.006	0.0014
	80	0.045	3.8	3.0	0.8	0.007	0.0018
	80	0.089	6.5	5.3	1.2	0.006	0.0013
	70	0.022	1.1	0.9	0.2	0.004	0.0009
	70	0.045	2.7	2.2	0.5	0.005	0.0011
	70	0.089	4.5	3.8	0.7	0.004	0.0008
2 (10.1)	100	0.045	8.7	6.7	2.0	0.015	0.0044
	80	0.045	5.7	4.6	1.1	0.010	0.0024
	80	0.089	8.3	6.7	1.6	0.008	0.0018
	70	0.045	2.5	2.1	0.4	0.005	0.0009
	70	0.089	4.2	3.5	0.7	0.004	0.0008
3 (16.3)	100	0.07	9.9	7.3	2.3	0.010	0.0032
	100	0.08	12.6	9.7	2.9	0.012	0.0036
	80	0.07	3.6	2.9	0.7	0.004	0.001
	80	0.13	4.9	4.0	0.9	0.003	0.0007
	80	0.27	11.1	9.0	2.1	0.003	0.0008
	70	0.07	1.3	1.1	0.2	0.0016	0.0003
	70	0.13	4.1	3.4	0.7	0.0026	0.0005
	70	0.13	4.1	3.4	0.7	0.0026	0.0005
4 (10.3)	100	0.09	9.5	7.3	2.2	0.008	0.0024
	80	0.09	2.4	1.9	0.5	0.002	0.0006
	80	0.18	8.0	6.5	1.5	0.004	0.0008
	70	0.05	0.8	0.66	0.13	0.0013	0.0003
	70	0.18	2.5	2.1	0.4	0.0012	0.0002

* The iron content in the catalyst (wt.%) is given in parentheses.

** Iron content in reaction mixtures.

for the samples tested. The results obtained are given below.

Sample	1	2	3	4
$E_2/\text{kJ mol}^{-1}$	44±4	44±4	64±6	68±6
$E_{-2}/\text{kJ mol}^{-1}$	57±4	57±4	77±7	82±8

It follows from the data in Table 3 that samples 1 and 2 with the iron content up to 10.1 wt.% show the highest catalytic activity. The rate constants decrease with an increase in the iron content to 16.3 wt.%. Sample 4 obtained at a higher temperature is less catalytically active than sample 2 with the same iron content (~10 wt.%) but prepared at a lower decomposition temperature. The most active catalysts (samples 1 and 2) are characterized by lower apparent activation energies: 44 and 57 kJ mol⁻¹ for the forward and backward isomerization reactions, respectively, which are rather low for the tested reaction. For the iron oxides of optimum composition supported on silica gel, these values are higher, being 53 and 69 kJ mol⁻¹, respectively.¹ For less active catalysts, the apparent activation energies increase and become equal to 64 and 77 kJ mol⁻¹ (sample 3) and 68 and 82 kJ mol⁻¹ (sample 4).

The specific catalytic activities of the iron-containing nanoparticles calculated from the initial reaction rates at 80 °C are presented below. When the iron content increases from 4.7 to 16.3 wt.% in samples 1–3 obtained under the same conditions, the specific catalytic activity passes through a maximum for the 10% metal content and further decreases. Sample 4 is less active.

Sample	[Fe] (wt.%)	A_{sp} /mole of product (mol Fe) ⁻¹ h ⁻¹
1	4.7	140
2	10.1	170
3	16.3	80
4	10.3	80

It is most likely that the differences in catalytic activity caused by an increase in the metal content in the sample and a change in the preparation conditions are related to specific features of the nanoparticle composition. The data presented in Table 1 show that the particle size changes insignificantly; however, the compositions of samples 1–4 differ substantially. It seems rather probable that the high catalytic activity of samples 1 and 2 is due to the Fe₃O₄ and γ-Fe₂O₃ oxides, whose structure is

close to spinel and which are present in the composition of the surface layers. These oxides include catalytically active mixed-charge states of metal^{II} and can participate in electron transfer in the key step of isomerization, as it has been proposed earlier.^{1,2} The high activity and the absence of the induction period on accumulating the isomerization products indicate that the catalytically active sites of the iron oxides stabilized on the UPTFE surface are accessible to reactants. Somewhat higher specific activity of sample 2 compared to sample 1 can be related, in particular, to a higher imperfectness of the particles.

The main reason for decreasing catalyst activity of the sample with a higher iron content (sample 3) can be the absence of γ -Fe₂O₃ in its composition. It follows from the known data¹ that α -Fe₂O₃ is less catalytically active. The synthesis at a higher temperature (sample 4) also provides a less active catalyst due to the formation of iron(II) oxide reduced to a higher extent and showing lower catalytic activity.¹ Another possible reason for a low activity of sample 4 is the absence of the iron fluoride phases. It has previously² been shown that the highest catalytic activity is characteristic of composites based on nanoparticles of iron(III) oxide and iron(II) chloride synthesized from iron(III) chloride. Probably, similar combination of iron oxides and fluoride in the same nanoparticle also favors catalysis.

Thus, the method proposed for the synthesis of iron oxide nanoparticles by the thermolysis of iron formate on the surface of the UPTFE stabilizing matrix provides the nanocomposites active in catalysis of chloroolefins. Multiphase nanoparticles, which are formed during the synthesis and in which some Fe^{III} ions are reduced to Fe^{II}, require no additional "activation" by reactants and perform isomerization without an induction period inherent in other catalytic systems based on iron oxides. Similarly to the iron oxides localized on the silica surface, the highest activity is characteristic of the highly defective samples including the γ -Fe₂O₃ phase. Their activity more than twofold exceeds that of the nanocomposites containing nanoparticles similar in size and composition but stabilized in the volume rather than on the surface of the polymeric polyethylene matrix.²

This work was financially supported by the Russian Foundation for Basic Research (Project Nos 05-03-32083, 03-03-33104, 04-03-32090, 04-03-32311, and 04-03-

32597), the International Scientific Technical Center (Grant 1991), the Russian Science Support Foundation, and the Division of Chemistry and Materials Science of the Russian Academy of Sciences (fundamental research programs "Fundamental Problems of Physics and Chemistry of Nanodimensional Systems and Materials" and "Directed Synthesis of Inorganic Substances with Specified Properties and Creation of Related Functional Materials").

References

1. T. N. Rostovshchikova, V. V. Smirnov, M. V. Tsodikov, O. V. Bukhtenko, Yu. V. Maksimov, O. I. Kiseleva, and D. A. Pankratov, *Izv. Akad. Nauk, Ser. Khim.*, 2005, 1376 [*Russ. Chem. Bull., Int. Ed.*, 2005, 1418].
2. T. N. Rostovshchikova, O. I. Kiseleva, G. Yu. Yurkov, S. P. Gubin, D. A. Pankratov, Yu. D. Perfil'ev, V. V. Smirnov, P. A. Chernavskii, and G. V. Pankina, *Vestn. Mosk. Gos. Univ., Ser. 2. Khim.*, 2001, **42**, 318 [*Vestn. Mosk. Univ., Ser. Khim.*, 2001 (Engl. Transl.)].
3. I. D. Kosobudskii and S. P. Gubin, *Vysokomol. Soedin.*, 1985, **27**, 689 [*Polym. Sci. USSR*, 1985, **27** (Engl. Transl.)].
4. S. P. Gubin, Yu. I. Spichkin, G. Yu. Yurkov, and A. M. Tishin, *Zh. Neorg. Khim.*, 2002, **47**, 32 [*Russ. J. Inorg. Chem.*, 2002, **47**, Suppl. 1 (Engl. Transl.)].
5. G. Yu. Yurkov, S. P. Gubin, D. A. Pankratov, Yu. A. Koksharov, A. V. Kozinkin, Yu. I. Spichkin, T. I. Nedoseikina, I. V. Pirog, and V. G. Vlasenko, *Neorg. Mater.*, 2002, **38**, 186 [*Inorg. Mater.*, 2002, **38** (Engl. Transl.)].
6. S. P. Gubin, M. S. Korobov, G. Yu. Yurkov, A. K. Tsvetnikov, and V. M. Buznik, *Dokl. Akad. Nauk*, 2003, **388**, 493 [*Dokl. Chem.*, 2003 (Engl. Transl.)].
7. M. S. Korobov, G. Yu. Yurkov, A. V. Kozinkin, Yu. A. Koksharov, I. V. Pirog, S. V. Zubkov, V. V. Kitaev, D. A. Sarychev, V. M. Buznik, A. K. Tsvetnikov, and S. P. Gubin, *Neorg. Mater.*, 2004, **40**, 31 [*Inorg. Mater.*, 2004, **40** (Engl. Transl.)].
8. S. J. Oh, D. C. Cook, and H. E. Townsend, *Hyperfine Interact.*, 1998, **112**, 59.
9. F. Menil, *J. Phys. Chem. Sol.*, 1985, **46**, 763.
10. E. G. Walton, D. B. Brown, H. Wong, and W. M. Reiff, *Inorg. Chem.*, 1977, **16**, 2425.
11. O. S. Morozova, Yu. V. Maksimov, D. P. Shashkin, P. A. Shirjaev, V. A. Zhorin, and O. V. Krylov, *Appl. Catal.*, 1991, **78**, 227.

*Received September 12, 2004;
in revised form April 6, 2005*